COMPDYN 2019
7th ECCOMAS Thematic Conference on
Computational Methods in Structural Dynamics and Earthquake Engineering
M. Papadrakakis, M. Fragiadakis (eds.)
Crete, Greece, 24–26 June 2019

DRIVE-BY DAMAGE MONITORING OF TRANSPORT INFRASTRUCTURE USING DIRECT CALCULATION OF THE PROFILE

J. Keenahan[1], E.J. OBrien[2], and Y. Ren[3]

[1] School of Civil Engineering, University College Dublin, Ireland
e-mail: jennifer.keenahan@ucd.ie

[2] School of Civil Engineering, University College Dublin, Ireland
e-mail: eugene.obrien@ucd.ie

[3] School of Civil Engineering, University College Dublin, Ireland
e-mail: ren.yifei@ucdconnect.ie

Abstract

Roads and railway tracks are a major focus of interest in transport infrastructure monitoring. Settlement in a road or railway track profile changes the dynamic excitation applied to passing vehicles. This, in turn, results in a changed dynamic response in the original source of loading, such as a passing vehicle. These changes in dynamic excitation make it possible to detect damage in transport infrastructure from the vehicle response. In this paper, the profile is calculated using accelerations in a passing vehicle and used to monitor transport infrastructure.

Keywords: Direct Integration, Drive-by, Profile, Railway Track, Acceleration, SHM.

1 INTRODUCTION

Roads and railway tracks are critical parts of transport infrastructure. They routinely become damaged with features emerging such as potholes in the roads and 'soft spots' in the railway track. These damages may influence the serviceable and safe operation of the transportation network. Therefore, infrastructure monitoring is an important area of research.

Railway tracks are subject to reductions in stiffness due to deteriorating foundations and to permanent fatigue deformations that result in a change in the track profile. The objective of this research is to identify local reductions of profile or stiffness that can help with the identification of problems related to track settlement, vehicle-ride comfort, track geometry and even ground-borne vibrations [1]. Railway track stiffness can currently be measured using specialised medium-speed vehicles or stationary equipment. A track recording vehicle (TRV) is a traditional method used by railway infrastructure managers to assess the condition of their network. A TRV is a specialised, instrumented train which periodically collects geometric data of the railway track including track gauge, longitudinal profile, alignment, super-elevation irregularity (cross level or cant) and twist. European Standard EN13848 defines the method of measurement of railway track using TRVs in Europe [2]. TRVs are the current preferred method of measurement for these parameters. However, they are expensive to operate and may disrupt regular services during operation. Using in-service vehicles to determine at least some of these parameters represents a possible alternative that can provide much more frequent measurements at much less cost [3].

In this method, sensors mounted on in-service vehicles collect accelerations and possibly other dynamic parameters. Improvements in band-width of wireless communications, reductions in sensor and data acquisition electronics cost have allowed the development of unattended track geometry inspection systems that are compact and robust enough to be mounted on in-service vehicles [4]. This concept of using trains in regular service to measure track stiffness has the potential to provide inexpensive daily 'drive-by' track monitoring to complement data collected by other less frequent (but more accurate) monitoring techniques.

Railway track longitudinal profile is also regard as indicator of serviceability condition. Perfectly level track profiles can minimise dynamic responses of the vehicle, which can increase passenger comfort, reduce power consumption and reduce wear on vehicle components. A reduction in vehicle dynamics also reduces the vehicle load on the track. Therefore, keeping a good vertical longitudinal profile helps maintain overall track condition through a reduction in vehicle dynamic effects [5].

Accelerometer(s) mounted on a vehicle also provide a way to measure road profile which is of low cost. González et al identify the relationship between vehicle accelerations and the power spectral densities of road surfaces using a transfer function [6]. The road condition is accurately classified by Fourier analysis which is used to calculate the power spectral density (PSD) function of the surface. OBrien et al present a drive-by method to monitor transport infrastructure (such as bridges and pavements) by analysing vehicle accelerations [7]. An algorithm is proposed to identify the dynamic vehicle-bridge interaction forces using the vehicle response. It is suggested that this method could be used to identify the global bending stiffness of the bridge and to predict the pavement roughness. This paper will use a new direct integration approach to calculate track and/or road profiles using vehicle accelerations. Points of low stiffness in the track are also determined as it is loaded track profile that is measured which is a combination of permanent deformation/profile and deflection in response to the weight of the train.

2 MODEL DESCRIPTION

2.1 Vehicle Model

The vehicle is represented by a 4 degree-of-freedom half-car model travelling on a beam-on-elastic-foundation track (Figure 1(a)) and rigid road (Figure 1(b)). The four independent degrees of freedom correspond to sprung mass bounce displacement, u_s, sprung mass pitch rotation θ_s and axle hop displacements of the unsprung masses at axles 1 and 2, u_{u1} and u_{u2} respectively. The vehicle body is represented by sprung mass, m_s. The axle components are represented by unsprung masses, m_{u1} and m_{u2}. The sprung mass connects to the axle masses via a combination of springs and dampers. The damping coefficients of viscous dampers are $C_{s,i}$ and stiffnesses of springs are $K_{s,i}$ which represent the suspension components for the front and rear axles ($i = 1,2$). The axle masses connect to the road or railway track surface via springs with linear stiffnesses, $K_{t,i}$ which represent the tyre components for the front and rear axles ($i = 1,2$). Finally, I_s is the sprung mass moment of inertia and the distances of the axles to the centre of gravity are D_1 and D_2. Table 1 gives the property values of the half-car.

Property	*Unit*	*Symbol*	*Half-Car and track model*	*Half-Car and road model*
Body mass	kg	m_s	16 200	16 200
Axle mass	kg	m_{u1}	700	700
		m_{u1}	1100	1100
Suspension stiffness	N/m	$K_{s,1}$	4×10^5	4×10^5
		$K_{s,2}$	1×10^6	1×10^6
Suspension damping	N s/m	$C_{s,1}$	1×10^4	1×10^4
		$C_{s,2}$	2×10^4	2×10^4
Tyre stiffness	N/m	$K_{t,1}$	1.75×10^6	1.75×10^6
		$K_{t,2}$	3.5×10^6	3.5×10^6
Pitch moment of inertia	kg m^2	I_s	111 193	93 457
Distance of axle to centre of gravity	m	D_1	4.13	2.375
		D_2	4.13	2.375

Table 1: Vehicle model properties.

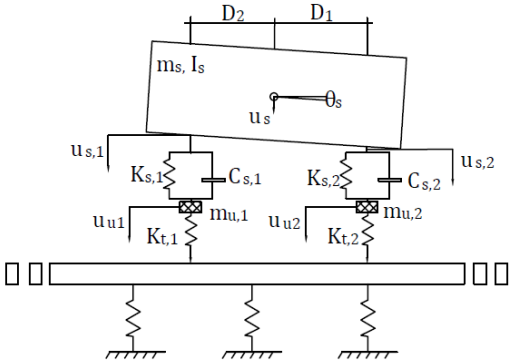

Figure 1(a): Half-Car and track model.

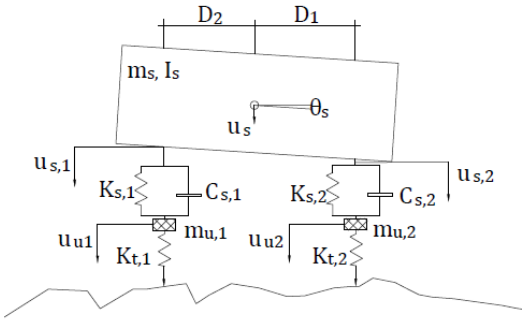

Figure 1(b): Half-Car and road model.

The equations of motion of the vehicle are obtained by imposing equilibrium of all forces and moments acting on the vehicle:

$$\mathrm{M}_v\ddot{u}_v + C_v\dot{u}_v + \mathrm{K}_v u_v = f_v \tag{1}$$

where M_v, C_v, and K_v are the mass, damping and stiffness matrices of the vehicle respectively. The vehicle accelerations, velocities and displacements are represented by vectors, $\ddot{u}_v$, $\dot{u}_v$ and u_v respectively, where the displacement vector of the vehicle is,

$$u_v = \{u_s, \theta_s, u_{u1}, u_{u2}\}^T \tag{2}$$

The time-varying dynamic interaction force vector is,

$$f_v = \{0,0,F_{t1},F_{t2}\}^T \tag{3}$$

The dynamic interaction force at wheel *i* is,

$$F_{ti} = K_{t,i} \times y_i \tag{4}$$

$i = 1,2$, where y_i is the road or track profile. The mass, damping and stiffness matrices are:

$$\mathrm{M_v} = \begin{bmatrix} m_s & 0 & 0 & 0 \\ 0 & I_s & 0 & 0 \\ 0 & 0 & m_{u,1} & 0 \\ 0 & 0 & 0 & m_{u,2} \end{bmatrix} \tag{5}$$

$$\mathrm{C_v} = \begin{bmatrix} C_{s,1}+C_{s,2} & D_1C_{s,1}-D_2C_{s,2} & -C_{s,1} & -C_{s,2} \\ D_1C_{s,1}-D_2C_{s,2} & {D_1}^2C_{s,1}+{D_2}^2C_{s,2} & -D_1C_{s,1} & D_2C_{s,2} \\ -C_{s,1} & -D_1C_{s,1} & C_{s,1} & 0 \\ -C_{s,2} & D_2C_{s,2} & 0 & C_{s,2} \end{bmatrix} \tag{6}$$

$$\mathrm{K_v} = \begin{bmatrix} K_{s,1}+K_{s,2} & D_1K_{s,1}-D_2K_{s,2} & -K_{s,1} & -K_{s,2} \\ D_1K_{s,1}-D_2K_{s,2} & {D_1}^2K_{s,1}+{D_2}^2K_{s,2} & -D_1K_{s,1} & D_2K_{s,2} \\ -K_{s,1} & -D_1K_{s,1} & K_{s,1}+K_{t,1} & 0 \\ -K_{s,2} & D_2K_{s,2} & 0 & K_{s,2}+K_{t,2} \end{bmatrix} \tag{7}$$

2.2 Road model

In this paper, a 100 m road profile is generated by Monte Carlo simulation according to the ISO standard [8]. It simulates a class 'A' road which is a 'very good' profile, typical of a well-maintained highway. The geometric spatial mean is 8×10^{-6} m^3/cycle. A moving average filter

is applied to the generated road profile heights, y_i. It is over a distance of 0.24 m to simulate the attenuation of short wavelength disturbances by the tyre contact patch [7,9].

2.3 Track Model

In past work, the railway track is represented using a beam-on-elastic-foundation model [1]. This model features a single layer of discrete elastic springs. Figure 1(a) shows the beam-on-elastic-foundation track model. It features an elastic beam (the rail) supported on some springs with different stiffness, k. Track supports have regular interval spacing, L_s, representing the spacing between the sleepers. A UIC60 rail is simulated as a finite element Euler-Bernoulli beam with one beam element per sleeper spacing. Each track element has 2 nodes with 2 degrees of freedom (DOF), vertical translation and rotation, at each node. Rail irregularities are not considered in this research which means the track profile is entirely from deflection of the springs under the loaded train.

3 DIRECT SOLUTION OF PROFILE CALCULATION

The forward problem and the inverse problem are features of any profile calculation. The forward problem is to find vehicle accelerations, velocities and displacements for a given profile. The inverse problem, in contrast, uses given $\ddot{u}$ and $\dot{\theta}_s$to find the profile. In previous research, the inverse problem is solved using a complex optimisation procedure [10]. It repeatedly solves the problem for thousands of trial profiles, until a good match is achieved between measured and theoretical accelerations. It also should repeat this for each segment of track/road. In this paper, the direct integration approach is proposed to solve the inverse problem directly to find the profile.

The forward problem is solved first. In the forward problem calculation, a 'true' profile is used to generate the 'measured' sprung mass accelerations and sprung mass pitch rotational velocity. Then, to test the method of solving the inverse problem, the profile y_i is calculated with these 'measured' sprung mass accelerations and sprung mass pitch rotational velocities. All problems are solved here using the Newmark-Beta integration scheme and simulated in MATLAB.

In the Newmark-Beta integration scheme, a value of γ=0.5 is used to ensure unconditional stability of the algorithm. In the Newmark-Beta method, the integration constants are chosen as:

$$\text{Time step } \Delta t,\ \ \gamma = 0.5, \beta = \ 0.25 \times (0.5 + \gamma)^2$$

$$a_0 = \frac{1}{\beta \times \Delta t^2},\ a_1 = \frac{\gamma}{\beta \times \Delta t},\ a_2 = \frac{1}{\beta \times \Delta t}, a_3 = \frac{1}{\beta \times 2} - 1, a_4 = \frac{\gamma}{\beta} - 1, \tag{8}$$

$$a_5 = \frac{\Delta t}{2} \times \left(\frac{\gamma}{\beta} - 2\right), a_6 = (1 - \gamma) \times \Delta t, a_7 = \ \gamma \times \Delta t$$

The profile is calculated step by step in the process as follows: The sprung mass bounce acceleration, $\ddot{u}$ and the sprung mass pitch rotational velocity, $\dot{\theta}_s$ are taken to be known at first. Then the sprung mass bounce displacement, u_s, and velocity, $\dot{u}_s$, sprung mass pitch rotational displacement, θ_s, and accelerations, $\ddot{\theta}_s$, can be calculated using the Newmark-Beta integration scheme:

$$u_{s,t+\Delta t} = (\ddot{u}_{s,t+\Delta t} + a_2 \times \dot{u}_{s,t} + a_3 \times \ddot{u}_{s,t})/a_0 + u_{s,t} \tag{9}$$

$$\dot{u}_{s,t+\Delta t} = \dot{u}_{s,t} + a_6 \times \ddot{u}_{s,t} + a_7 \times \ddot{u}_{s,t+\Delta t} \tag{10}$$

$$\theta_{s,t+\Delta t} = (\dot{\theta}_{s,t+\Delta t} + a_4 \times \dot{\theta}_{s,t} + a_5 \times \ddot{\theta}_{s,t})/a_1 + \theta_{s,t} \quad (11)$$

$$\ddot{\theta}_{s,t+\Delta t} = a_0 \times (\theta_{s,t+\Delta t} - \theta_{s,t}) - a_2 \times \dot{\theta}_{s,t} - a_3 \times \ddot{\theta}_{s,t} \quad (12)$$

According to Equations (1) to (7), the equations of motion of the sprung mass can be found:

$$m_s \times \ddot{u}_{s,t+\Delta t} + (C_{s,1} + C_{s,2}) \times \dot{u}_{s,t+\Delta t} + (D_1 C_{s,1} - D_2 C_{s,2}) \times \dot{\theta}_{s,t+\Delta t} - C_{s,1} \times \dot{u}_{u1,t+\Delta t} - C_{s,2} \times \dot{u}_{u2,t+\Delta t} + (K_{s,1} + K_{s,2}) \times u_{s,t+\Delta t} + (D_1 K_{s,1} - D_2 K_{s,2}) \times \theta_{s,t+\Delta t} - K_{s,1} \times u_{u1,t+\Delta t} - K_{s,2} \times u_{u2,t+\Delta t} = 0 \quad (13)$$

$$I_s \times \ddot{\theta}_{s,t+\Delta t} + (D_1 C_{s,1} - D_2 C_{s,2}) \times \dot{u}_{s,t+\Delta t} + ({D_1}^2 C_{s,1} + {D_2}^2 C_{s,2}) \times \dot{\theta}_{s,t+\Delta t} - D_1 C_{s,1} \times \dot{u}_{u1,t+\Delta t} + D_2 C_{s,2} \times \dot{u}_{u2,t+\Delta t} + (D_1 K_{s,1} - D_2 K_{s,2}) \times u_{s,t+\Delta t} + ({D_1}^2 K_{s,1} + {D_2}^2 K_{s,2}) \times \theta_{s,t+\Delta t} - D_1 K_{s,1} \times u_{u1,t+\Delta t} + D_2 K_{s,2} \times u_{u2,t+\Delta t} = 0 \quad (14)$$

The terms, $\dot{u}_{u2,t+\Delta t}$ and $u_{u2,t+\Delta t}$ can be removed by combining Equations (14) with Equations (13), scaled by D_2:

$$D_2 m_s \times \ddot{u}_{s,t+\Delta t} + D_2(C_{s,1} + C_{s,2}) \times \dot{u}_{s,t+\Delta t} + D_2(D_1 C_{s,1} - D_2 C_{s,2}) \times \dot{\theta}_{s,t+\Delta t} + D_2(K_{s,1} + K_{s,2}) \times u_{s,t+\Delta t} + D_2(D_1 K_{s,1} - D_2 K_{s,2}) \times \theta_{s,t+\Delta t} + I_s \times \ddot{u}_{s,t+\Delta t} + (D_1 C_{s,1} - D_2 C_{s,2}) \times \dot{u}_{s,t+\Delta t} + ({D_1}^2 C_{s,1} + {D_2}^2 C_{s,2}) \times \dot{\theta}_{s,t+\Delta t} + (D_1 K_{s,1} - D_2 K_{s,2}) \times u_{s,t+\Delta t} + ({D_1}^2 K_{s,1} + {D_2}^2 K_{s,2}) \times \theta_{s,t+\Delta t} = (D_2 C_{s,1} + D_1 C_{s,1}) \times \dot{u}_{u1,t+\Delta t} + (D_2 K_{s,1} + D_1 K_{s,1}) \times u_{u1,t+\Delta t} \quad (15)$$

In the Newmark-Beta method,

$$\dot{u}_{u1,t+\Delta t} = a_1 \times (u_{u1,t+\Delta t} - u_{u1,t}) - a_4 \times \dot{u}_{u1,t} - a_5 \times \ddot{u}_{u1,t} \quad (16)$$

Substituting (16) into (15), the unsprung mass displacement can be calculated:

$$u_{u1,t+\Delta t} = (D_2 m_s \times \ddot{u}_{s,t+\Delta t} + I_s \times \ddot{\theta}_{s,t+\Delta t} + (D_2 C_{s,1} + D_1 C_{s,1}) \times \dot{u}_{s,t+\Delta t} + (D_2 D_1 C_{s,1} + {D_1}^2 C_{s,1}) \times \dot{\theta}_{s,t+\Delta t} + (D_2 K_{s,1} + D_1 K_{s,1}) \times u_{s,t+\Delta t} + (D_2 D_1 K_{s,1} + {D_1}^2 K_{s,1}) \times \theta_{s,t+\Delta t} + (D_2 C_{s,1} + D_1 C_{s,1}) \times (a_1 \times u_{u1,t} + a_4 \times \dot{u}_{u1,t} + a_5 \times \ddot{u}_{u1,t}))/(D_2 K_{s,1} + D_1 K_{s,1} + (D_2 C_{s,1} + D_1 C_{s,1}) \times a_1) \quad (17)$$

Unsprung mass acceleration and velocity can be calculated using the Newmark-Beta method:

$$\ddot{u}_{u1,t+\Delta t} = a_0 \times (u_{u1,t+\Delta t} - u_{u1,t}) - a_2 \times \dot{u}_{u1,t} - a_3 \times \ddot{u}_{u1,t} \quad (18)$$

$$\dot{u}_{u1,t+\Delta t} = \dot{u}_{u1,t} + a_6 \times \ddot{u}_{u1,t} + a_7 \times \ddot{u}_{u1,t+\Delta t} \quad (19)$$

This is used to calculate $f_{v,t+\Delta t}$ at time step, $t + \Delta t$,

The effective stiffness matrix is:

$$\bar{K} = K_v + a_0 \times M_v + a_1 \times C_v \quad (20)$$

The effective force is:

$$\bar{f}_{v,t+\Delta t} = \bar{K} \times u_{v,t+\Delta t} \quad (21)$$

and,

$$f_{v,t+\Delta t} = \bar{f}_{v,t+\Delta t} - \mathrm{M}_v \times (a_0 \times u_{v,t} + a_2 \times \dot{u}_{v,t} + a_3 \times \ddot{u}_{v,t}) - C_v \times (a_1 \times u_{v,t} + a_4 \times \dot{u}_{v,t} + a_5 \times \ddot{u}_{v,t}) \quad (22)$$

According to Equation (3), $f_{v,t+\Delta t} = \{0,0,F_{t1,t+\Delta t},F_{t2,t+\Delta t}\}^T$, so $F_{ti,t+\Delta t}$ is known, and the profile can be found according to Equation (4):

$$y_{i,t+\Delta t} = F_{ti,t+\Delta t}/K_{t,i} \tag{23}$$

The calculated road profile and track profile are shown in the Figure 2(a) and Figure 2(b) respectively. The results show that the profiles are found with a great degree of accuracy. This direct integration approach allows the calculation to be completed in a very short time which is massively more efficient than an optimisation approach.

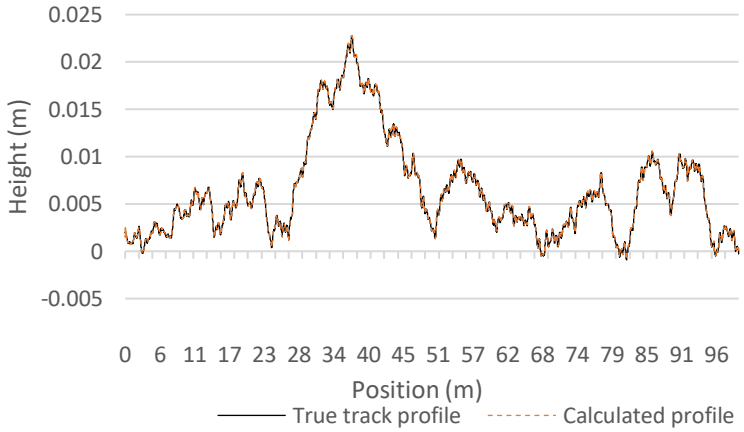

Figure 2(a): Calculated road profile and true profile.

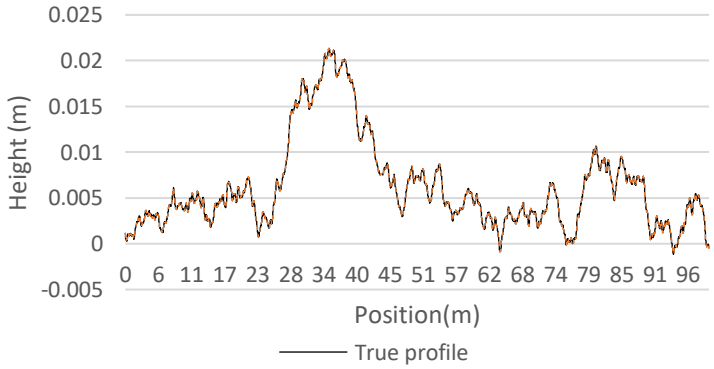

Figure 2(b): Calculated track profile and true profile.

4 DAMAGE IN RAILWAY TRACK

Local variations in the track stiffnesses can be detected from the calculated track profile which is effectively a combination of profile and deformations under load. In this example, there is a 50% loss in the track stiffness from 60 m to 65 m. This changes the 'measured' accelerations and rotational velocities. Using these changed signals, the new deflected profiles are calculated. The calculated track profile with and without a local reduction in railway track stiffness are shown in Figure 3. The results show that calculating track profile is a good means of identifying defects in the track.

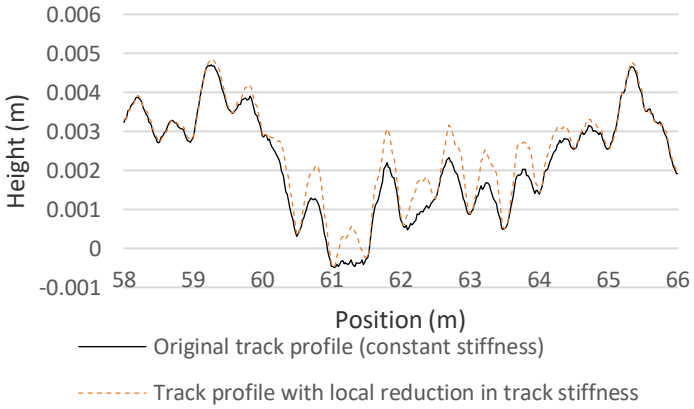

Figure 3: Calculated track profile with variations in railway track stiffness.

5 CONCLUSIONS

This paper introduces a new method of monitoring transport infrastructure. A direct integration approach is proposed to calculate road and railway track profiles using measured accelerations from vehicles. The direct method is used to calculate profiles using these 'measured' accelerations. The results show that the calculated profiles are the same as the 'true' profiles which are from the forward problem (used to generate the accelerations). What is more, direct integration is much more efficient and allows the calculation to be completed much more quickly in comparison to the optimisation procedure used by previous researchers. Also, the calculated track profile can be used to detect local variations in railway track stiffness. It has good potential as a means of detecting areas where railway tracks have suffered a reduction in stiffness.

ACKNOWLEDGMENTS

Mr. Yifei Ren acknowledges the Ph.D. scholarship received jointly from University College Dublin and the China Scholarship Council.

REFERENCES

[1] P. Quirke, D. Cantero, E. J. OBrien, C. Bowe, Drive-by detection of railway track stiffness variation using in-service vehicles. *Proceedings of the Institution of Mechanical Engineers, Part F: Journal of Rail and Rapid Transit*, **231**, 498-514, 2017.

[2] IS EN 13848: Railway Applications - Track - Track Geometry Quality - CEN European. Committee for Standardisation.

[3] E. J. OBrien, C. Bowe, P. Quirke, and D. Cantero, Determination of longitudinal profile of railway track using vehicle-based inertial readings. *Proceedings of the Institution of Mechanical Engineers, Part F: Journal of Rail and Rapid Transit*, **231**, 518-534, 2017.

[4] P. Weston, C. Roberts, G. Yeo, E. Stewart, Perspectives on railway track geometry condition monitoring from in-service railway vehicles. *Vehicle System Dynamics*, **53**, 1063-1091, 2015.

[5] R. D. Frohling, Deterioration of railway track due to dynamic vehicle loading and spatially varying track stiffness. PhD Thesis, University of Pretoria, South Africa, 1997.

[6] A. González, E. J. OBrien, Y. Y. Li, K. Cashell, The use of vehicle acceleration measurements to estimate road roughness. *Vehicle System Dynamics*, **46**(6), 483-499, 2008.

[7] E. J. OBrien, P. J. McGetrick, A. González, A drive-by inspection system via vehicle moving force identification. *Smart Structures and Systems*, **13**(5), 821-848, 2014.

[8] ISO 8608: Mechanical vibration-road surface profiles - reporting of measured data, 1995

[9] N. K. Harris, E. J. OBrien, A. González, Reduction of bridge dynamic amplification through adjustment of vehicle suspension damping. *Journal of Sound and Vibration*, **302**(3), 471-485, 2007.

[10] E. J. OBrien, J. Keenahan, Drive-by damage detection in bridges using the apparent profile'. *Structural Control and Health Monitoring*, **22**(5), 813-825, 2015.